UMYU Scientifica, Vol. 4 NO. 4, December 2025, Pp 122 – 136
https://doi.org/10.56919/usci.2544.011
ISSN: 2955 – 1145 (print); 2955 – 1153 (online)
A periodical of the Faculty of Natural and Applied Sciences, UMYU, Katsina

ORIGINAL RESEARCH ARTICLE

Computational Elucidation of 4-Amino-N-(4-aminophenyl)benzamide Adsorption and Corrosion Inhibition on Mild Steel Using a Multi-Level Quantum–Simulation Approach

Abosede Adejoke Badeji*
Department of Chemical Sciences, Tai Solarin Federal University of Education, Ijebu Ode, Ogun State, Nigeria

ABSTRACT

In this study, the corrosion inhibition performance of 4-amino-N-(4-aminophenyl)benzamide (DOF) on the Fe (110) surface was investigated using density functional theory (DFT), quantum theory of atoms in molecules (QTAIM), non-covalent interaction (NCI) analysis, and Monte Carlo (MC) simulations. This study represents the first integrated theoretical investigation of DOF adsorption on the Fe(110) surface, using quantum-topological and surface-simulation techniques to the best of our knowledge. DFT studies on the structure were performed at the B3LYP/6-31+G(d,p)//SMD(H_2O) level of theory to elucidate the electronic properties, quantum descriptors and charge distribution. Electronic structure results revealed that DOF possesses a high-lying HOMO, low chemical hardness, and strong global softness, indicating a strong tendency to donate electrons to the Fe (110) surface. QTAIM and NCI analyses confirmed the presence of mixed electrostatic and weak covalent interactions involving the amino and amide functional groups, which stabilise the adsorption process. MC simulations further demonstrated the thermodynamic favorability of DOF adsorption, with a total energy of -127.65 kcal/mol, an adsorption energy of -165.16 kcal/mol, and a minimal deformation energy of 0.29 kcal/mol, indicating a stable, spontaneous interaction without significant structural distortion. These combined computational results show that DOF forms a strongly adsorbed, protective molecular layer on Fe(110) in aqueous media, making it a promising candidate for corrosion inhibition applications. The molecular insights obtained here not only clarify its inhibition mechanism but also provide a theoretical foundation for future studies on designing even more efficient benzamide-based corrosion inhibitors.

ARTICLE HISTORY

Received June 12, 2025
Accepted December 28, 2025
Published December 30, 2025

KEYWORDS

Corrosion inhibitor, Mild steel, DFT, NCI, QTAIM, Monte Carlo Simulation.

INTRODUCTION

Carbon steels remain indispensable in industrial sectors due to their excellent mechanical strength, affordability, and ease of fabrication. Despite these advantages, their long-term reliability is severely compromised by corrosion, particularly when exposed to aggressive environments such as acidic media, high salinity, or atmospheric pollutants (Bender et al., 2022; Odeyemi & Alaba, 2025; Schlegel, 2023). Among the wide range of corrosion mitigation strategies, the use of organic corrosion inhibitors stands out as one of the most practical, cost-effective, and efficient approaches (Anadebe et al., 2025; Azeez et al., 2024; Badeji, 2025). Organic inhibitory molecules typically contain heteroatoms such as N, O, S, and π-conjugated systems (aromatic rings, double bonds, or electron-rich substituents) that facilitate adsorption onto metal surfaces (Ebenso et al., 2021; Murmu et al., 2022; Schlegel, 2023). The formation of a stable, adherent protective film at the metal-solution interface is widely accepted as the principal mechanism by which these inhibitors slow down corrosion processes (Taghavikish et al., 2017). However, despite extensive research, the microscopic origins of inhibition, particularly how subtle modifications in molecular geometry or electronic structure drastically influence efficiency, remain insufficiently understood.

Although experimental techniques such as weight-loss measurements, electrochemical impedance spectroscopy (EIS), potentiodynamic polarisation, SEM, FTIR, and X-ray structural analysis provide valuable macroscopic performance metrics, they are often time-consuming, expensive, and limited in their ability to reveal the underlying molecular-level interactions responsible for inhibition (Ebenso et al., 2021; Murmu et al., 2022). Consequently, modern corrosion science increasingly leverages computational chemistry to elucidate inhibitor behaviour at the atomic scale. Density Functional Theory (DFT) offers deep insight into the electronic structure,

Correspondence: Abosede Adejoke Badeji. Department of Chemical Sciences, Tai Solarin Federal University of Education, Ijebu Ode, Ogun State, Nigeria. ✉ ogunlanaaa@tasued.edu.ng.
How to cite: Badeji, A. A. (2025). Computational Elucidation of 4-Amino-N-(4-aminophenyl)benzamide Adsorption and Corrosion Inhibition on Mild Steel Using a Multi-Level Quantum–Simulation Approach. *UMYU Scientifica*, 4(4), 122 – 136. https://doi.org/10.56919/usci.2544.011

global reactivity descriptors, charge distribution, and adsorption propensity of corrosion inhibitors (Mamand et al., 2024). These descriptors, such as chemical hardness, softness, electronegativity, dipole moment, and Fukui functions, have proven indispensable in evaluating inhibition performance and predicting molecular reactivity trends. Complementarily, Monte Carlo and molecular dynamics simulations provide a realistic model of inhibitor adsorption in the presence of solvent molecules, ionic species, and thermal fluctuations, overcoming the limitations of vacuum-phase theoretical calculations (Heard et al., 2019; Mamand et al., 2024; Murmu et al., 2022).

While numerous studies have addressed thiourea derivatives (Hegazy et al., 2023; Jiang et al., 2024), benzamides (Mishra et al., 2018a; Muthamma et al., 2021), and amino-substituted aromatics as effective inhibitors (Oyeneyin et al., 2022; Zhang et al., 2020), the molecule in the present study, 4-amino-N-(4-aminophenyl)benzamide (DOF), remains insufficiently explored, particularly with respect to its adsorption behaviour on mild steel surfaces in aqueous corrosive conditions. Also, numerous benzamide derivatives investigated previously have mainly focused on monofunctional or weakly substituted systems, with limited mechanistic analysis beyond global reactivity descriptors. In particular, the influence of dual para-aminosubstitution on electronic delocalisation, multidentate surface anchoring, and adsorption thermodynamics has not been systematically explored. This made DOF a molecule of interest as it is structurally distinct in this regard. It combines an amide linkage with two electron-donating amino groups embedded within a conjugated aromatic framework. This architecture is expected to enhance both σ-donation through heteroatoms and π–d interactions with iron surfaces. Moreover, from a methodological perspective, many existing computational corrosion studies on benzamides rely solely on isolated DFT descriptors or surface simulations, often leading to descriptive rather than mechanistic conclusions. This present study addresses this gap by integrating Quantum Theory of Atoms in Molecules (QTAIM), Non-Covalent Interaction (NCI), and a Monte Carlo simulation workflow, among others, to investigate the anticorrosive potential of DOF on the Fe(110) surface. This integrative approach enables a complete understanding of its structural reactivity, adsorption thermodynamics, intermolecular interactions, and surface-protection mechanisms. The results is expected to provide fundamental insights not accessible by conventional experimentation and support the rational design of next-generation organic corrosion inhibitors.

COMPUTATIONAL METHODS

2.1 Density functional theory methods

In this study, first-principles quantum-chemical calculations were performed to investigate the structural, electronic, and reactive properties of 4-amino-N-(4-aminophenyl)benzamide (DOF). All density functional theory (DFT) computations were performed using the *Gaussian 16* program package (Frisch et al., 2016). Geometry optimisations were performed in the gas phase, without symmetry constraints, to locate the most stable conformers. The B3LYP hybrid functional, which combines Becke's three-parameter exchange with the Lee-Yang-Parr correlation (Becke, 1993), was employed due to its established accuracy for predicting molecular geometries, electron density distribution, and reactivity characteristics of organic inhibitors (Cho et al., 2015). The 6-31+G(d,p) basis set was employed to provide a balanced description of valence, polarisation, and diffuse functions, which are necessary for reliable modelling of heteroatom-containing corrosion inhibitor molecules (Fouda & Besley, 2018). This level of theory has been widely validated for organic corrosion inhibitors and provides a reliable balance between accuracy and computational cost for molecular electronic descriptors (Carranza et al., 2021; Fatemeh Mollaamin & Majid Monajjemi, 2023). Frequency analyses were performed to confirm the absence of imaginary frequencies, ensuring that the optimised structures correspond to true minima on the potential energy surface. To improve relevance to aqueous corrosion environments, the solvent effects were incorporated using the universal implicit Solvation Model based on Density (SMD) with water as the solvent (Marenich et al., 2009). Quantum chemical descriptors, including energy gap (ΔE), chemical hardness (η), softness (S), chemical potential (μ), electrophilicity index (ω), and electronegativity (χ), were evaluated in both phases (gas and aqeous) from HOMO-LUMO energies based on Koopmans' approximation (Badeji et al., 2025; Koopmans, 1934), as follows:

$$\Delta E = E_{LUMO} - E_{HOMO} \quad (1)$$

$$\eta = \frac{E_{LUMO} - E_{HOMO}}{2} \quad (2)$$

$$\delta = \frac{1}{2\eta} \quad (3)$$

$$\mu = -\frac{IP + EA}{2} \quad (4)$$

$$\omega = \frac{\mu^2}{2\eta} \quad (5)$$

The HOMO-LUMO plots were generated using Chemcraft software (Zhurko & Zhurko, 2005), while OriginLab (Moberly et al., 2018) was used for density-of-states (DOS) analysis. Natural bond orbital (NBO) analysis was employed to gain insight into the electronic perturbation, and was computed using equation 6 (Weinhold, 2012).

$$E^{(2)} = \Delta E^2_{ij} = qi\frac{(Fi,j)^2}{(Ej - Ei)} \quad (6)$$

Where qi denotes the electron donor orbital occupancy, ε_i and ε_j stand for the orbital energies of the donor and acceptor NBO orbitals. Further electronic and interaction-types analyses, including Molecular Electrostatic Potential (MESP), Quantum Theory of Atoms in Molecules (QTAIM) topology, and Non-Covalent Interaction (NCI) index, were conducted using Multiwfn 3.7 (Lu & Chen, 2012) with a fine real-space grid (spacing ≤ 0.1 bohr) and default convergence thresholds,

and the results were visualised in VMD 1.9.3 (Humphrey et al., 1996). The virial theorem, as expressed in equations **7** and **8**, was employed to establish the relationship between the electron energy density and the Laplacian of the electron density in QTAIM (Popelier, 2016).

$$\frac{1}{4}\nabla^2\rho_{(r)} = 2G_{(r)} + V_{(r)} \qquad 7$$

$$G_{(r)} + V_{(r)} = H_{(r)} \qquad 8$$

It should be noted that DFT calculations were restricted to the isolated inhibitor molecule; explicit metal–surface interactions were treated separately using Monte Carlo simulations, avoiding methodological inconsistencies associated with cluster-based Fe modelling in Gaussian.

2.2 Monte Carlo Simulation Method

To complement the DFT results, the adsorption behaviour of DOF on a mild steel surface (Fe (110)) was examined using the Monte Carlo (MC) simulation method implemented in the Materials Studio software package (Meunier & Robertson, 2021). The Fe(110) facet was selected due to its thermodynamic stability and frequent exposure in corrosion environments, as widely reported in both experimental and theoretical studies (Badeji, 2025; Liao et al., 2022a; Mishra et al., 2018b; Othman et al., 2025). Before simulation, the geometries of DOF, water, and hydroxonium ions were optimised using the Forcite module with the Universal Force Field (UFF) to ensure reliable structural inputs (Anadebe et al., 2025; A. Badeji, 2025). The Universal Force Field (UFF) was adopted due to its demonstrated applicability to aromatic amides and metal–organic interfaces (Boyd et al., 2017). The mild steel substrate was modelled by cleaving the Fe(110) surface into five atomic layers, and a 30 Å vacuum slab was introduced along the z-direction to eliminate spurious interactions between periodic images. To replicate a corrosive aqueous medium, the simulation cell was solvated with 80 water (H_2O) molecules, 10 hydroxonium (H_3O^+) ions, and 10 chloride (Cl^-) ions, representing acidic aqueous conditions commonly employed in corrosion experiments.

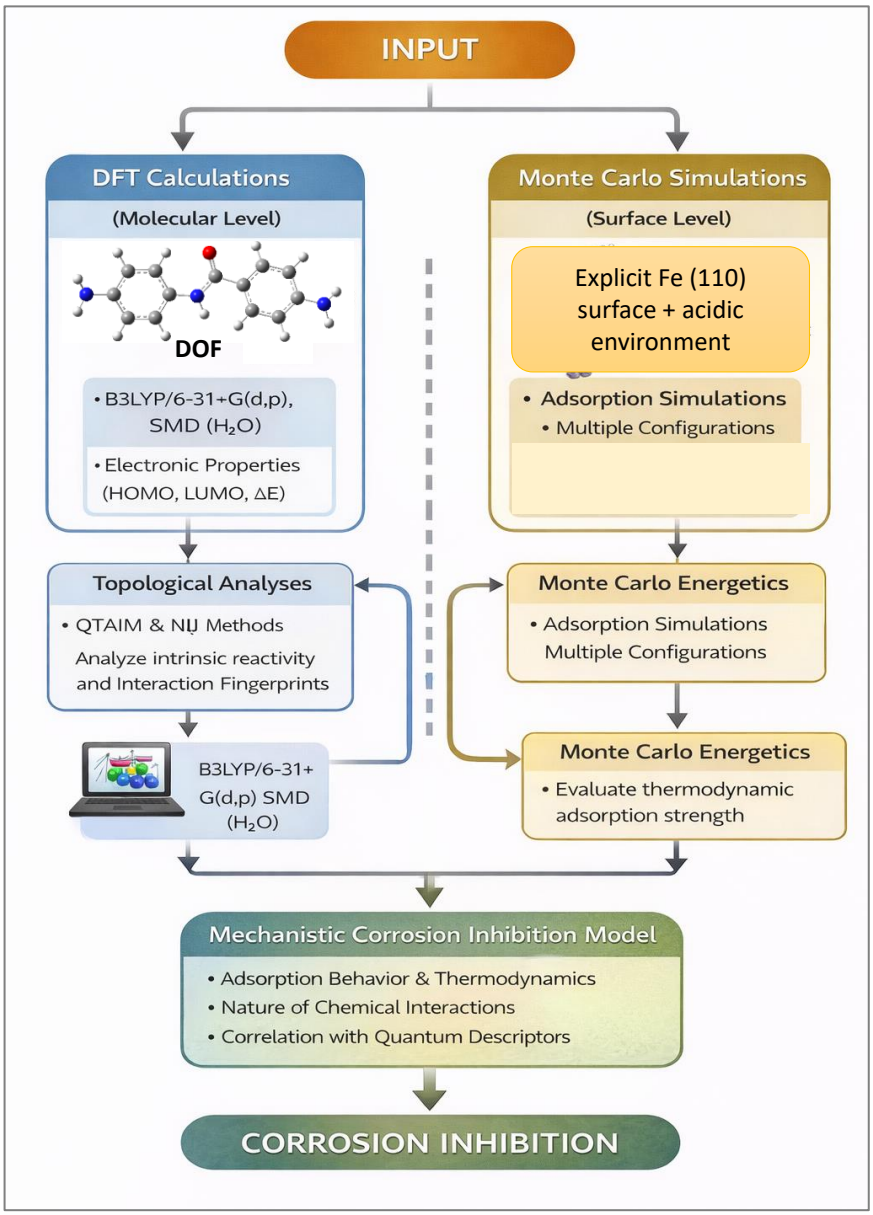

Figure 1: Workflow illustrating the separation and complementarity of molecular DFT and surface Monte Carlo simulation employed in this study

Table 1: Summary of computational settings employed in this study

Method	Parameter	Setting
DFT	Software	Gaussian 16
	Functional	B3LYP
	Basis set	6-31+G(d,p)
	Solvent model	SMD (H_2O)
	Geometry convergence	Default Gaussian tight criteria.
QTAIM/NCI	Software	Multiwfn 3.7
	Grid spacing	≤ 0.1 bohr
	Density cutoff	1×10^{-6} a.u.
Monte Carlo Simulation	Software	Materials Studio
	Force field	UFF
	Surface model	Fe(110), 5 layers
	Ensemble	NVT
	Temperature	298 K
	Simulation time	100 ps

The MC calculations were carried out using the quench molecular dynamics approach (Gelb & Müller, 2002) under the canonical (NVT) ensemble at 298 K, with a quench molecular dynamics protocol (initial 50 ps equilibration) prior to production MC sampling (100 ps). Adsorption configurations were generated and subsequently analyzed in terms of total adsorption energy, rigid adsorption energy, and deformation energy, thereby providing insights into the stability and interaction strength of DOF on the Fe(110) surface.

Figure 1 presents a schematic workflow illustrating the separation and complementarity of the molecular-level density functional theory (DFT) calculations and surface-level Monte Carlo (MC) simulations employed in this study. DFT-based analyses were restricted to the isolated inhibitor molecule to extract intrinsic electronic reactivity, charge-transfer capability, and non-covalent interaction fingerprints, while MC simulations explicitly modelled adsorption on the Fe(110) surface in a corrosive aqueous environment. This dual-level strategy avoids the methodological inconsistencies associated with cluster-based metal modelling in quantum calculations and enables a coherent mechanistic interpretation by linking electronic structure descriptors to thermodynamically stable adsorption behaviour. The summary table for the computational studies employed in this study is shown in Table 1 below.

RESULTS AND DISCUSSION

3.1 Structural Analysis of 4-amino-N-(4-aminophenyl)benzamide

The structural geometry of the 4-amino-N-(4-aminophenyl)benzamide (DOF) system revealed characteristic bond lengths and angles consistent with those of conjugated aromatic amide derivatives. As depicted in Table 2, the amide linkage in DOF shows a C_{11}-O_{12} bond length of 1.232 Å, a value shorter than the typical C-O single bond (1.43 Å) but in line with C=O double bond character (1.20-1.23 Å) (Axthammer et al., 2016; Kalwar et al., 2022). This confirms strong π-character in the carbonyl moiety, a feature critical for electron donation and back-donation with transition metal d-orbitals during adsorption (Jay et al., 2025; Krosschell et al., 2024). The adjacent C_{11}-N_{13} bond length of 1.376 Å reflects partial double bond character due to resonance delocalisation between the carbonyl oxygen and amide nitrogen, further stabilising conjugation with the aromatic ring. The C_{15}-N_{13} bond (1.415 Å) and C_{22}-N_{25} bond (1.403 Å) correspond to aryl-amine linkages, slightly elongated compared to a free aromatic C-N (~1.36 - 1.38 Å) (Adrion & Lopez, 2022). The C_6-N_{28} bond (1.390 Å) lies within the expected range for an aniline-type substituent, indicating conjugation of the -NH_2 lone pair with the benzene ring, which enhances the donor capability of N_{28} toward Fe d-states (Oliveira et al., 2017). The N-H bonds (H_{14}-N_{13} = 1.009 Å; H_{26}-N_{25} = 1.011 Å) are typical for sp^2-hybridised amines, reinforcing that no abnormal elongation or weakening occurs upon optimisation.

Bond angles further reveal the electronic environment of the active sites. At the amide nitrogen (N_{13}), the C_{15}-N_{13}-C_{11} angle of 129.115° and the H_{14}-N_{13}-C_{11} angle of 116.170° demonstrate a clear sp^2 hybridisation, which aligns with resonance delocalisation across the amide. The smaller C_{15}-N_{13}-H_{14} angle (114.572°) supports slight pyramidalization, maintaining reactive lone-pair density on N_{13} for adsorption. Within the carbonyl moiety, the C_3-C_{11}-O_{12} angle of 121.398° and the complementary C_3-C_{11}-N_{13} angle of 115.547° are nearly trigonal planar, confirming delocalized π-bonding across the amide group. The planar arrangement enhances conjugation between the aromatic backbone and the amide functionality, thereby improving surface anchoring and charge transfer when interacting with Fe(110). At the terminal amino substituents, the C_6-N_{28}-H_{29} angle of 117.020° and the C_{22}-N_{25}-H_{26} angle of 115.338° both approximate sp^2-hybridisation. These values suggest that the -NH_2 groups are not purely pyramidal (sp^3) but instead partially delocalized with the aromatic π-system. This delocalisation stabilises the molecule while keeping the nitrogen lone pairs accessible for coordination chemistry. This structural result of DOF after optimisation underscores the inhibitory potential on Fe(110). The shortened C=O bond and partial double-bond character of C-N linkages highlight strong electron delocalisation, ensuring efficient orbital overlap with Fe surface d-states. Moreover, the availability of three nitrogen donor sites (N_{13}, N_{25}, N_{28}) and one oxygen donor site (O_{12}) provides

multiple anchoring points for chemisorption. The near-planar amide environment further facilitates parallel alignment of the aromatic rings with the Fe(110) surface, thereby enabling additional π- π interactions.

Table 2: The structural parameters showing results of the before and after optimisation of the bond length and bond angles of DOF calculated at the DFT/B3LYP/631+G(d,p) level of theory.

SYSTEM	Bond Labels	Bond Length (Å)	Bond Labels	Bond Angles (°)
DOF	$C_{22} – N_{25}$	1.403	$C_{15} – N_{13} – H_{14}$	114.572
	$C3 – C_{11}$	1.498	C_{15} - $N_{13} – C_{11}$	129.115
	$C_{11} – O_{12}$	1.232	H_{14} - $N_{13} – C_{11}$	116.170
	$C_6 – N_{28}$	1.390	$C_3 – C_{11} – O_{12}$	121.398
	$C_{15} – N_{13}$	1.415	$C_3 – C_{11} – N_{13}$	115.547
	$H_{14} – N_{13}$	1.009	$C_3 – C_{11} – O_{12}$	120.766
	$C_{11} – N_{13}$	1.376	$C_6 – N_{28} – H_{29}$	117.020
	$H_{26} – N_{25}$	1.011	$C_{22} – N_{25} – H_{26}$	115.338

Table 3. Energies of HOMO (eV), LUMO (eV), HOMO-LUMO energy gap (Egap) (eV), Chemical Softness (σ, eV), hardness (η, eV), chemical potential (μ, eV), and electrophilicity index (ω, eV) calculated using the DFT/B3LYP/6-31+G(d,p) level of theory.

SYSTEM	HOMO/eV	LUMO/eV	Energy gap(eV)	σ(eV)	η(eV)	μ(eV)	ω(eV)
DOF (gas)	-5.24	-1.03	4.21	0.24	2.10	-3.14	2.34
DOF (H_2O)	-5.31	-1.14	4.16	0.24	2.08	-3.23	2.50

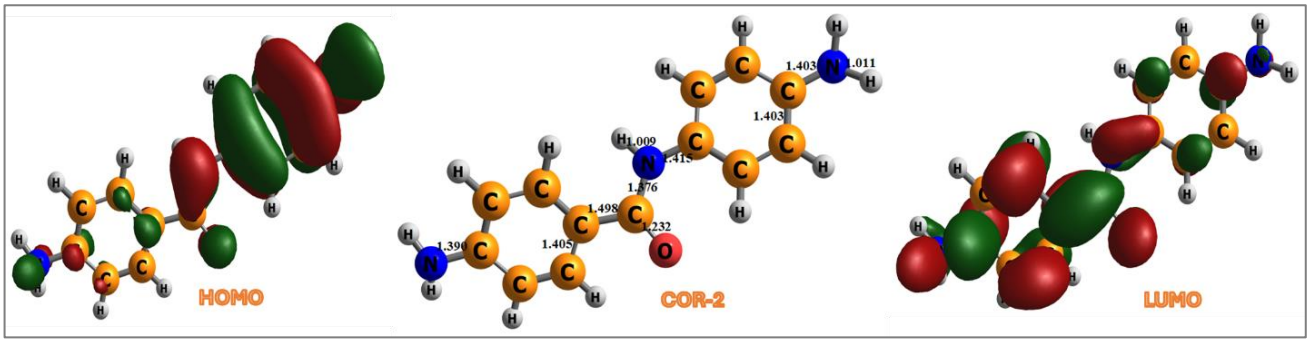

Figure 2. The structural presentation of DOF, the Molecular orbital (MO) isosurface map showing its highest occupied molecular orbitals (HOMO) and lowest unoccupied molecular orbital (LUMO) at the DFT/B3LYP/631+G(d,p) level of theory.

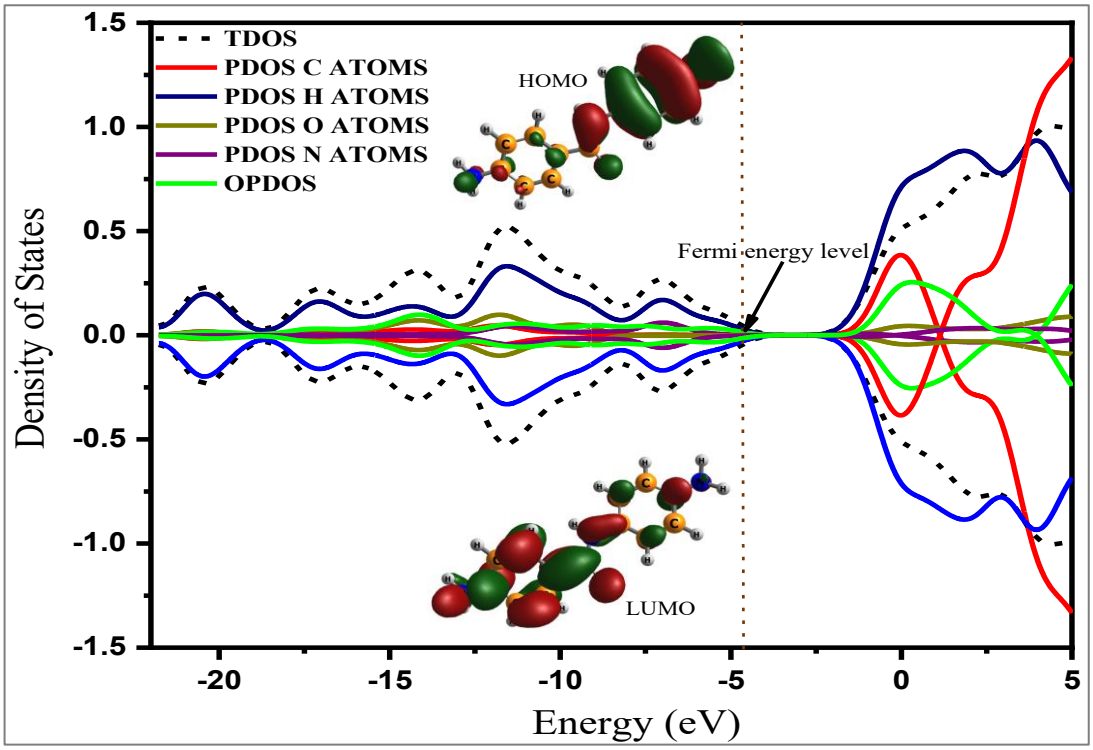

Figure 3. Density of States (DOS) plots for the 4-amino-N-(4-aminophenyl)benzamide (DOF) system, depicting the distribution of electrons and electronic orbital contributions at distinct quantum states.

Table 4. Tabulated NBO results of 4-amino-N-(4-aminophenyl)benzamide showing the donor and acceptor orbital transitions, occupancy, and energies studied at the DFT/B3LYP/631+G(d,p) level of theory.

SYSTEM	Donor (i)	Occupancy	Acceptor (j)	Occupancy	$E^{(2)}$ (kcal/mol)	E(j)-E(i) a.u	F(i,j) a.u
DOF	π^*C_{15} - C_{16}	0.423	π^*C_{17} - C_{20}	0.343	287.21	0.01	0.083
	π^*C_1 - C_6	0.407	π^*C_4 - C_5	0.301	212.06	0.01	0.079
	π^*C_{11} - O_{12}	0.329	π^*C_2 - C_3	0.405	92.67	0.02	0.065

3.2 Reactivity Analysis of DOF

3.2.1 Frontier Molecular Orbital (FMO) Analysis

The frontier molecular orbital (FMO) analysis was performed to evaluate the electronic properties of DOF and its tendency to interact with the Fe(110) surface. The computed highest occupied molecular orbital (HOMO), lowest unoccupied molecular orbital (LUMO), and associated quantum descriptors are presented in Table 3. DOF exhibits a HOMO energy of -5.24 eV and a LUMO energy of -1.03 eV in gas phase, corresponding to an energy gap (ΔE) of 4.21 eV. Meanwhile, the values of these parameters in the solvent phase are -5.31 eV, -1.14 eV, and 4.16 eV for HOMO, LUMO, and ΔE, respectively. From Figure 2, the LUMO is mainly located on the nitrobenzene substituent on the carbonyl group, while the HOMO is mainly located on the nitrobenzene substituent on the amine group. From these values, the chemical hardness (η), softness (σ), chemical potential (μ), and electrophilicity index (ω) were calculated using Koopmans' approximation according to equations 1-5 (Bhatia, 2024; Kaya, 2025; Oladipo et al., 2025). The results indicate η = 2.10 eV, σ = 0.24 eV, μ = -3.14 eV, and ω = 2.34 eV for the gas phase and η = 2.08 eV, σ = 0.24 eV, μ = -3.23 eV, and ω = 2.50 eV for the solvent phase. The moderate HOMO-LUMO energy gap suggests that DOF maintains thermodynamic stability while still possessing sufficient reactivity to interact with metallic centres. The relatively high hardness (2.10/2.08 eV) and low softness (0.24 eV) categorise DOF as a moderately hard species, suggesting that its interaction with Fe(110) is likely to be localised and site-specific, dominated by electron donation from heteroatoms. The chemical potential value of -3.14/-3.23 eV reflects the ability of DOF to donate electron density toward the partially filled Fe 3d orbitals, particularly through the amide oxygen and amino nitrogen atoms (Zainab et al., 2024). Moreover, the electrophilicity index of 2.34/2.50 eV indicates a balanced donor-acceptor character, allowing for both σ-donation from lone pairs and π-backdonation from Fe d-states into the vacant orbitals of DOF. These results suggest that DOF could adsorb on Fe(110) primarily via multidentate coordination involving the amide O and amino N atoms, reinforced by π-d interactions from the conjugated aromatic rings (Hamidi et al., 2024; Le Minh Pham et al., 2022). The dual donor-acceptor nature of the molecule will promote strong anchoring to the Fe surface, thereby forming a protective layer that hinders electron-transfer processes associated with corrosion.

3.2.2 Density of States (DOS) Analysis

The Density of states (DOS) analysis is a powerful tool to probe the electronic structure of organic inhibitors and their interaction potential with metallic surfaces. DOS reveals the distribution and relative contributions of atomic orbitals across a wide energy spectrum (Ebenso et al., 2021; El-Hendawy et al., 2022; Nelson et al., 2025). This allows for the identification of the specific atoms and orbitals that dominate near the Fermi level, which is critical for understanding adsorption behaviour (Badeji et al., 2026; Fung et al., 2021; Liao et al., 2022). In corrosion inhibition studies, overlapping states of heteroatoms at the metal surface near the Fermi level indicate strong orbital hybridisation. At the same time, the spatial localisation of the HOMO and LUMO provides further insight into donor-acceptor interactions. According to Figure 3, the TDOS profile shows significant orbital contributions around the Fermi level, highlighting the availability of electronic states for surface interactions. Decomposition of the PDOS reveals that carbon (red) and hydrogen (blue) atoms dominate the DOS at higher energies, while oxygen (green) and nitrogen (purple) atoms make pronounced contributions near the frontier orbital region, consistent with their role as the principal adsorption centres. The HOMO distribution (inset, upper) is localised mainly over the amide nitrogen, carbonyl oxygen, and adjacent aromatic carbons. This localisation underscores the strong donor capacity of the heteroatoms, which are expected to coordinate with Fe(110) surface atoms via σ-donation. In contrast, the LUMO (inset, lower) is delocalized across the conjugated aromatic system, enabling π-backdonation from Fe d-states into the molecular framework. This dual localization pattern suggests that DOF can act both as an electron donor and acceptor during adsorption, thereby stabilizing the molecule–surface interaction. The alignment of the HOMO energy (-5.24 eV) just below the Fermi level (-5.0 eV dotted line) confirms the molecule's tendency to donate electron density to Fe orbitals, while the accessible LUMO (-1.03 eV) permits charge acceptance, supporting a donor-acceptor interaction mechanism. This interpretation is consistent with the global reactivity descriptors, which indicated a moderate energy gap (4.21 eV) and balanced electrophilicity (ω = 2.34 eV). Furthermore, the overlapping PDOS contributions of O and N atoms with the TDOS in the vicinity of the Fermi level suggest strong orbital hybridization, reinforcing their role as active centers for chemisorption.

3.2.3 Natural Bond Orbital (NBO) Analysis

To gain further insight into the intramolecular charge delocalisation and stabilisation of DOF, natural bond orbital (NBO) second-order perturbation analysis was performed, as depicted in Table 4. Three dominant donor-acceptor interactions were identified for this study (Lu et al., 2024; Rai Deka et al., 2024). This analysis was employed to elucidate the intramolecular charge delocalisation and donor-acceptor interactions in DOF,

providing a quantum chemical perspective on its reactivity (Demir et al., 2016).

Table 5. The Quantum theory of atoms in molecules (QTAIM) results of 4-amino-N-(4-aminophenyl)benzamide at the bond critical points

Interaction type	Bonds	CP	$\rho(r)$	$\nabla^2\rho^{(r)}$	$G_{(r)}$	$K_{(r)}$	$V_{(r)}$	$H_{(r)}$	$G_{(r)}/V_{(r)}$	ELF	ε	λ_1	λ_2	λ_3
Vander Waals interaction	$H_{14} - H_8$	38	0.012	0.054	0.011	-0.003	-0.008	0.003	-1.375	0.026	1.86	-0.01	-0.003	0.067
Electrostatic/Hydrogen bond	$H_{21} - O_{12}$	65	0.018	0.062	0.015	-0.001	-0.014	0.001	-1.071	0.057	0.095	-0.019	-0.018	0.099

Positive $\nabla^2\rho^{(r)}$ values confirm closed-shell, noncovalent interactions, $G_{(r)}/V_{(r)} \approx 1$ indicates hydrogen bonding, while values > 1 indicate weak dispersive (van der Waals) interactions.

In DFT calculations, NBO analysis provides deeper insights into localised electron density redistribution within the molecule. Specifically, second-order stabilisation energies ($E^{(2)}$) quantify the extent to which filled bonding orbitals donate electron density into neighbouring antibonding orbitals, thereby revealing resonance effects, conjugation pathways, and the relative strength of electronic interactions (Demir et al., 2016; Lu et al., 2024; Rai Deka et al., 2024). In corrosion inhibition studies, these electronic delocalisations are particularly important because they influence the molecule's electron-donating capability, polarizability, and adsorption affinity toward the metallic surface. Herein, the strongest interaction occurs between $\pi^*(C_{15}\text{-}C_{16}) \rightarrow \pi^*(C_{17}\text{-}C_{20})$, with an exceptionally high stabilisation energy of 287.21 kcal/mol. This interaction reflects robust π-π conjugation between adjacent phenyl fragments, extending delocalisation across the aromatic scaffold. The large E^2 value and the minimal orbital gap indicate that these orbitals are nearly degenerate and strongly coupled, thereby enhancing electronic polarizability and providing an efficient pathway for electron redistribution (Mancuso et al., 2020). A similarly strong stabilization is observed for $\pi^*(C_1\text{-}C_6) \rightarrow \pi^*(C_4\text{-}C_5)$, with $E^{(2)}$ of 212.06 kcal/mol. This again highlights pronounced delocalisation across the aromatic rings, confirming that DOF possesses a highly conjugated backbone that can act as a charge reservoir. The third notable interaction, $\pi^*(C_{11}\text{-}O_{12}) \rightarrow \pi^*(C_2\text{-}C_3)$ with $E^{(2)}$ of 92.67 kcal/mol, demonstrates significant resonance between the amide carbonyl group and the adjacent aromatic system. This conjugation corroborates the shortened C=O bond length observed in the geometry optimisation and indicates partial delocalisation of the carbonyl π-electrons. This result confirms that DOF is electronically stabilised by a network of strong $\pi^* \rightarrow \pi^*$ forward transitions, with an additional resonance involving the amide carbonyl. These features endow the molecule with both localised donor sites (amide O and amino N atoms) and an extended conjugated system that can engage in π-d orbital coupling with Fe(110), supporting its role as a highly efficient corrosion inhibitor.

3.3 Electronic Interaction Analysis

3.3.1 Quantum theory of Atoms in molecules (QTAIM)

To quantify weak intramolecular contacts that can influence adsorption and film formation, Richard Bader's quantum theory of atoms in molecules (QTAIM) analysis was performed (Mojica-Sánchez, 2023). QTAIM provides a framework for characterising the nature and strength of intra- and intermolecular interactions from electron density distributions, and selected bond critical point (BCP) parameters as reported in Table 5**.** For each BCPs at H_{14}-H_8 and H_{21}-O_{12}, the electron density ρ(r), Laplacian $\nabla^2\rho(r)$, kinetic energy density $G_{(r)}$, potential energy density $V_{(r)}$, total energy density $H_{(r)}$, the ratio $G_{(r)}/V_{(r)}$, the electron localization function (ELF), ellipticity (ε), and the eigenvalues of the Hessian matrix [50] were reported. According to reports, when the electron density at the

BCPs gives $\rho^{(r)} < 0.02$ a.u. with positive Laplacian values ($\nabla^2 \rho^{(r)} > 0$), it suggests that the interactions are primarily closed-shell in nature, dominated by weak van der Waals and electrostatic forces (Bakheit et al., 2023; Martín Pendás & Contreras-García, 2023). The H_{14}-H_8 contact is characterised by a very low electron density (ρ = 0.012 a.u.) and a positive Laplacian ($\nabla^2 \rho$ = 0.054 a.u.), together with a small, positive total energy density of 0.003 a.u. The H_{21}-O_{12} contact displays somewhat larger electron density (ρ = 0.018 a.u.) and a slightly higher Laplacian ($\nabla^2 \rho$ = 0.062 a.u.), with the total energy density remaining marginally positive ($H_{(r)}$ = 0.001 a.u.).

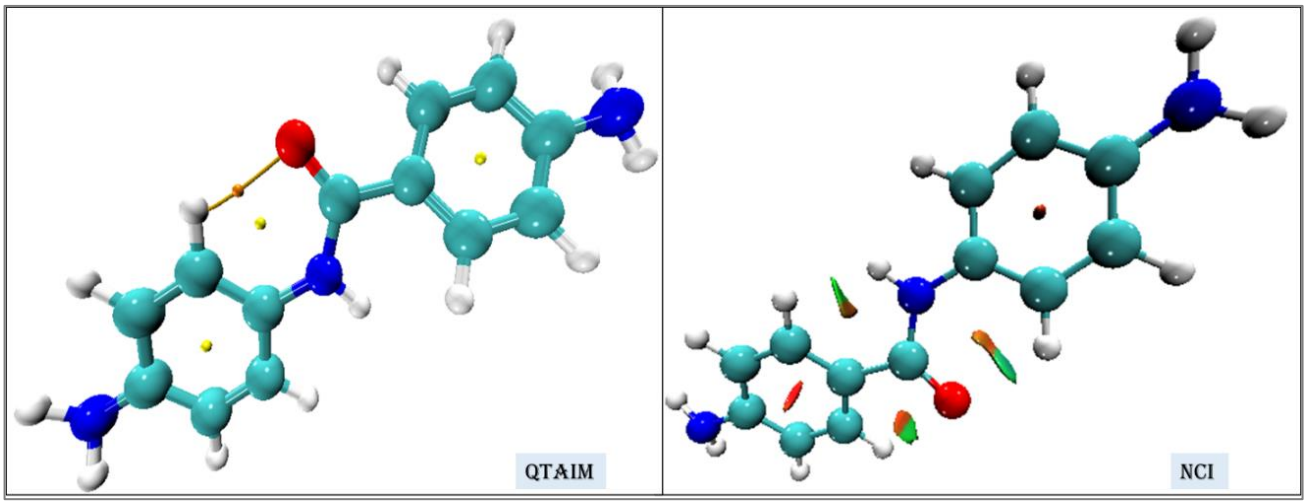

Figure 4: Presentation of the Quantum Theory of Atoms in Molecules (QTAIM) and the non-covalent interactions (NCI) plots of the studied 4-amino-N-(4-aminophenyl)benzamide corrosion inhibitor material.

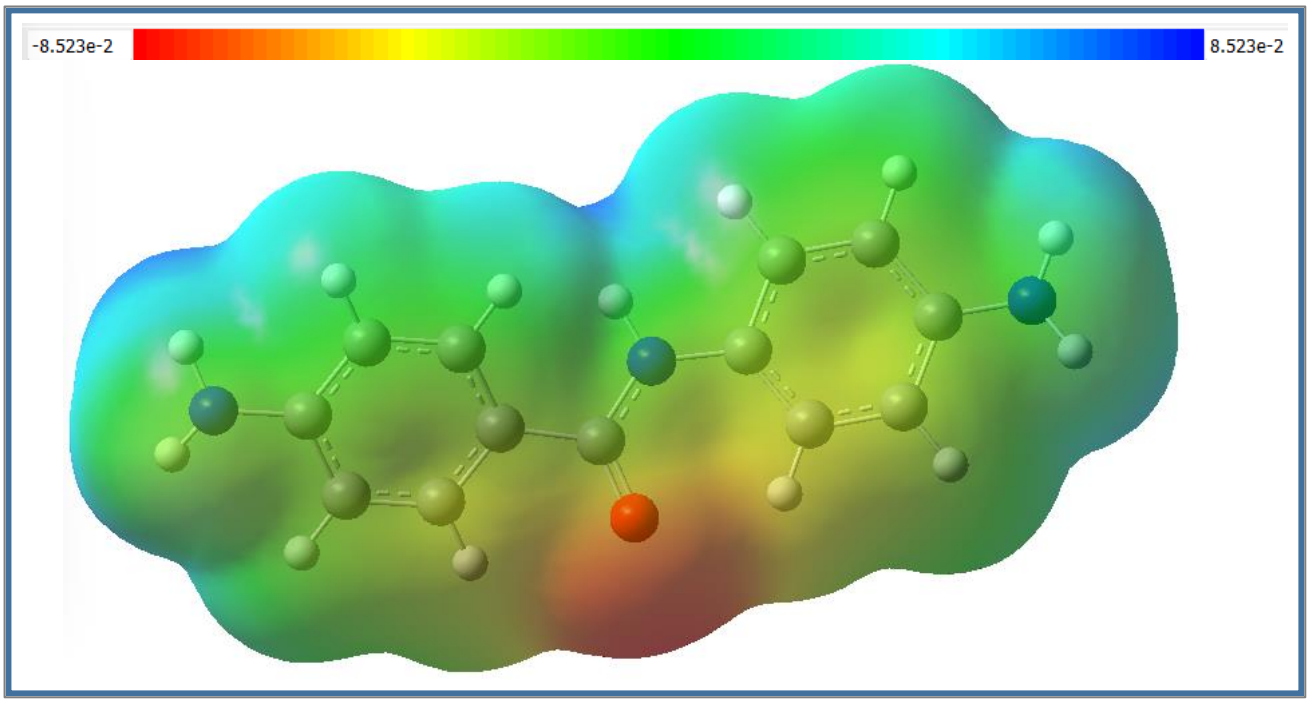

Figure 5: The Molecular Electrostatic Potential (MESP) isosurface map distribution of the 4-amino-N-(4-aminophenyl)benzamide corrosion inhibitor material showing areas of electron delocalisation.

These signatures are diagnostic of a closed-shell, noncovalent interaction (typical of weak H···H contacts or van der Waals contacts) as will be revealed in the NCI analysis. The low ELF of 0.026 and 0.057 and the small magnitude of the potential energy density ($V_{(r)}$) of -0.008 and -0.014 a.u further confirm that the interaction is weak and chiefly electrostatic/dispersion in character. Hence, the QTAIM data indicate that DOF is stabilised by weak intramolecular noncovalent interactions, with the H_{21}-O_{12} contact being the more significant of the two examined. Furthermore, from an adsorption/corrosion perspective, it is essential to note that the partial localisation of electron density at O_{12} (and at amine N sites from other analyses) enhances their effectiveness as σ-donor sites to Fe surface atoms, facilitating the formation of an ordered, adherent inhibitor layer on Fe(110).

3.3.2 Non-Covalent Interaction (NCI) Analysis

The NCI plots of DOF (Figure 4) provide detailed insights into the weak interactions that stabilise the inhibitor's geometry and potentially enhance its

adsorption on the Fe(110) surface. The reduced density gradient (RDG) isosurfaces and colored regions illustrate the presence of non-covalent interactions such as hydrogen bonding, van der Waals forces, and steric effects. The green isosurfaces correspond to weak but stabilising van der Waals interactions, which play a significant role in modulating DOF's conformational flexibility (Tsuji et al., 2025; Zheng et al., 2020). The red patches reveal steric repulsions, mostly localised around the aromatic rings and adjacent hydrogen atoms, suggesting regions of electron density crowding (Bakheit et al., 2023; Martín Pendás & Contreras-García, 2023). This observation suggests that π-π stacking interactions could contribute to the adsorption of DOF onto the Fe(110) surface. Overall, the coexistence of stabilising hydrogen bonds, van der Waals interactions, and π-π delocalisation provides a strong electronic rationale for the effective surface anchoring of DOF, complementing results from DOS, QTAIM, and Monte Carlo simulations.

3.3.3 Molecular Electrostatic Potential (MESP) Analysis

The MESP surface of DOF, as reported in Figure 5, reveals the electronic distribution and possible reactive sites responsible for adsorption on the Fe(110) surface. The colour scheme ranges from red (electron-rich, nucleophilic regions) to blue (electron-deficient, electrophilic regions) (Haritha & Suresh, 2024). From the figure, the red zones are mainly localised around the oxygen atoms (C=O, -OH) and the nitrogen atoms of the amine groups, indicating regions of high electron density. These sites are expected to act as strong electron donors and serve as anchoring points for coordination with vacant d-orbitals of Fe atoms during adsorption. Conversely, the blue regions are concentrated around hydrogen atoms bonded to electronegative elements (-NH, -OH), representing electropositive areas that can interact with electron-rich centres of the metal surface or neighbouring inhibitor molecules through hydrogen bonding (Badeji et al., 2024; Kumar et al., 2023; Oladipo et al., 2023). The aromatic π-systems also display moderately negative potential regions, suggesting the possibility of π-metal interactions or π-π stacking, which further stabilise adsorption. This dual nature enhances both chemisorption and physisorption, supporting the trends observed in QTAIM and NCI analyses.

3.4 Monte Carlo Molecular Dynamics (MD) Simulation

To complement the quantum chemical analyses, Monte Carlo (MC) simulations were employed to investigate the adsorption configuration and interaction strength of the inhibitor on the Fe(110) surface in a simulated corrosive environment (Kasprzhitskii & Lazorenko, 2021). This approach provides a molecular-level understanding of how the inhibitor competes with water molecules, hydronium (H_3O^+) ions, and chloride (Cl^-) ions for active adsorption sites (Wang et al., 2025). By visualising the spatial arrangement and adsorption behaviour, the MC simulation offers valuable insight into the stability and protective efficiency of the inhibitor film on the mild steel surface (Othman et al., 2016). Hence, the adsorption configuration of the inhibitor on the Fe(110) surface within a simulated aqueous corrosive environment is illustrated in Figure 6. The system contains water molecules, hydronium ions (H_3O^+), and chloride ions (Cl^-), mimicking realistic acidic conditions. Simulation results, as depicted in Table 6, show that the total energy of the system was found to be -127.65 kcal/mol, while the adsorption energy of the inhibitor was calculated as -165.16 kcal/mol, indicating a strong and energetically favourable interaction with the metallic surface (Azeez et al., 2024; Wang et al., 2025). The rigid adsorption energy (-165.45 kcal/mol), being slightly more negative than the adsorption energy, suggests minimal structural reorganisation of the inhibitor upon adsorption. This observation is further supported by the very low deformation energy (0.29 kcal/mol), signifying that the inhibitor maintains structural integrity during surface binding. These results confirm the strong affinity and stability of the inhibitor film on the steel surface, consistent with effective corrosion inhibition performance. The adsorption configuration also implies that the inhibitor can form a stable protective layer on the steel surface, thereby impeding the ingress of corrosive ions (Cl^-, H_3O^+). The balance between chemisorption (via heteroatoms and π-electrons) and physisorption (via van der Waals and electrostatic forces) contributes to the film's stability.

Table 6. Molecular dynamics simulation results for the 4-amino-N-(4-aminophenyl)benzamide corrosion inhibitor on the the Fe(110) surface.

Parameters	Values (kcal/mol)
Total Energy	-127.65
Adsorption Energy	-165.16
Rigid adsorption energy	-165.45
Deformation energy	0.29

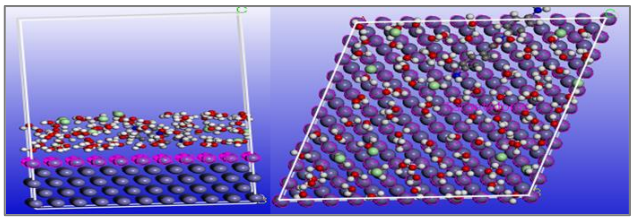

Figure 6: Top and front view of the Monte Carlo molecular dynamics corrosion inhibition simulation of 4-amino-N-(4-aminophenyl)benzamide corrosion inhibitor material on Fe(110) surface in different mediums.

3.5 Mechanistic Correlation of Quantum Descriptors and Adsorption Behaviour

To move beyond a descriptive approach, the electronic descriptors, topological analyses, and surface simulation results are integrated and interpreted within a unified corrosion inhibition mechanism. Frontier molecular orbital localisation identifies the amide oxygen (O) and amino nitrogen (N) atoms as dominant electron-donor sites, enabling σ-donation to vacant Fe 3d orbitals. This is

corroborated by QTAIM analysis, which classifies key interactions as predominantly closed-shell with partial covalent character, indicating a mixed physico-chemical adsorption mechanism. NCI isosurfaces further reveal extended green regions around the aromatic rings and heteroatoms, highlighting dispersion-driven stabilisation and π–d interactions that promote parallel alignment of DOF on the Fe(110) surface. These molecular-scale features directly translate into the large negative adsorption energy observed in Monte Carlo simulations, demonstrating how intrinsic electronic structure governs macroscopic inhibition performance.

Table 7: Comparative benchmarking of DOF with reported benzamide-based corrosion inhibitors

	Functional Groups	ΔE (eV)	Adsorption Energy (kcal/mol)	Reference
N-phenyl benzamide	Amide	2.97 – 4.60	−150.8 to −211.5	Mishra et al. (2018)
Benzamide derivative	Amide, thioamide, C=S, -SO_2NH_2	5.56 – 6.37	-215.6 to −220.6	(Iravani et al., 2025).
Amino-benzamide derivative	Amide, –NH_2	4.53 – 5.02	−128.1 to −141.3	(Boughoues et al., 2020)
Thiourea derivative	Amide, –NH_2, –C=S	3.91 -3.96	−67.17	(Hegazy et al., 2023)
Benzimidazole derivatives	imidazole	6.53 – 7.58	−43.5 to −71.8	(Mamand et al., 2023)
DOF (this work)	Amide, –NH_2	**−4.16**	**−165.16**	This work

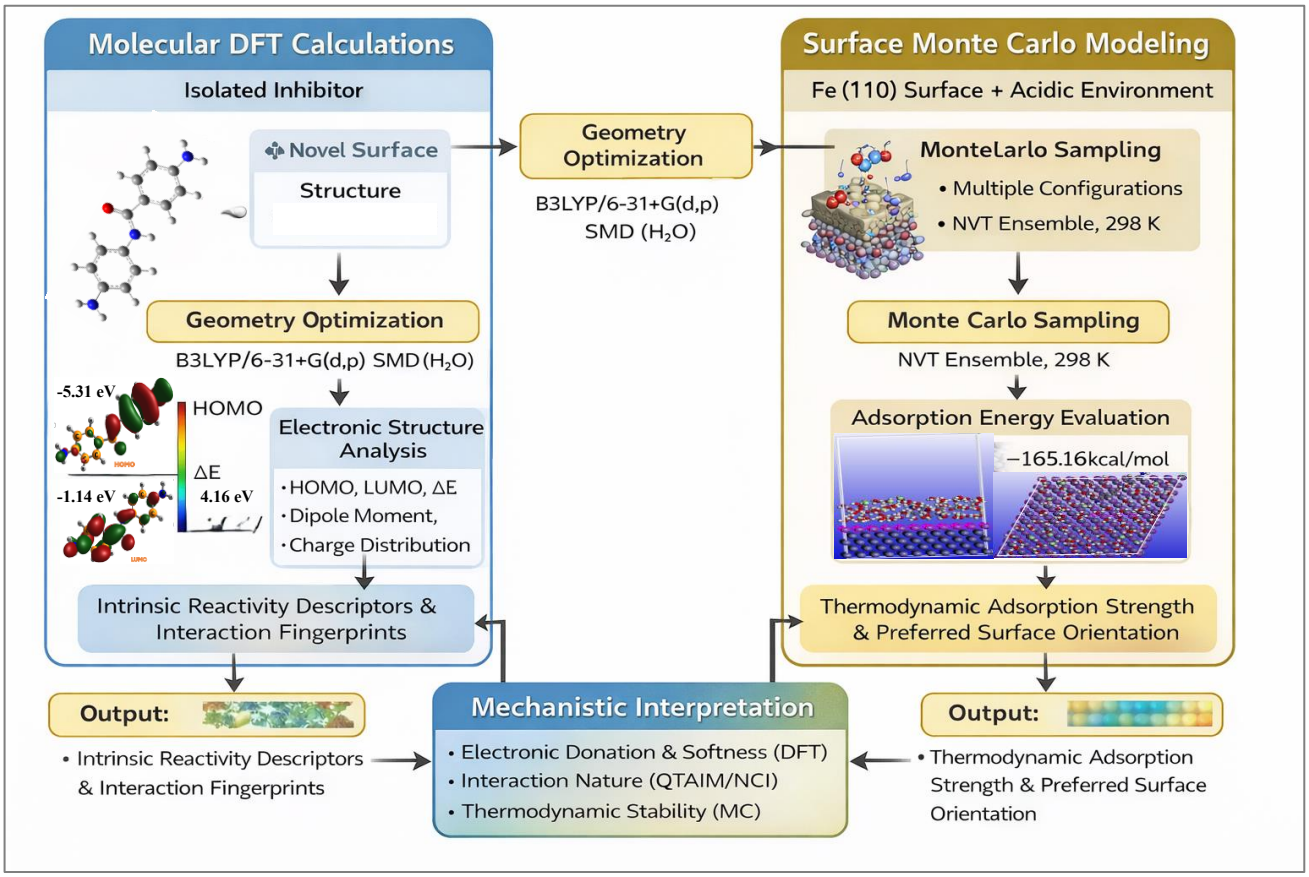

Figure 7: Workflow diagram to illustrate the separation and complementarity of molecular DFT and surface MC simulation.

To contextualise the inhibition potential of DOF, its key quantum descriptors and adsorption energy were benchmarked against representative benzamide-based inhibitors reported in the literature (Table 7). It is important as this comparison helps place the inhibition potential of DOF in the context of isolated descriptor analysis and assess whether the molecular design approach followed in this study can be reflected in the actual adsorption benefits or not. Electronically speaking, the intrinsic reactivity energy and charge-transfer ability of the inhibitors are reflected in the reported ΔE. Benzimidazole derivatives have the highest ΔE (6.53–7.58 eV), indicating relatively low molecular softness and a decreased probability of donating electrons to the metal surface. These compounds exhibit the lowest adsorption energies (-43.5 to -71.8 kcal/mol), indicating that, in these cases, weak physisorption with only restricted surface interactions predominates.

Although thiourea derivatives have functional groups of sulfur (C=S), which have been shown to exhibit high affinity to metals, thiourea derivatives show moderate

values of ΔE (3.91 -3.96 eV) but relatively low values of adsorption energy (-67.17 kcal/mol). This difference shows that the mere presence of heteroatoms may not necessarily result in strong adsorption, but effective inhibition arises from the cooperative interactions among electronic delocalisation, functional group accessibility, and the planar nature of the molecules. Amino-benzamide derivatives show intermediate behaviour, with ΔE values in the range of 4.53–5.02 eV and adsorption energies of -128.1 to -141.3 kcal/mol. When amino substituents are introduced, electron donation increases relative to unsubstituted systems, leading to a stronger adsorption strength.

Nevertheless, the monosubstituted nature of these molecules limits multidentate surface anchoring and π-electron delocalisation. However, significantly, N-phenyl benzamide and multifunctional benzamide derivatives with thioamide and sulfonamide functional groups exhibit a wide range of adsorption energies, with at least some having adsorption energies below -200 kcal/mol. Although these values would imply robust interactions on the surface, the wide ΔE ranges (2.97–4.60 eV and 5.56–6.37 eV, respectively) indicate a high degree of variability in the electronic stability and reactivity, which could be due to either the rigidity or the steric effects on the structure or the limited conjugation needed to adjust the adsorption process.

Interestingly, DOF is evidenced to have a balanced and optimised inhibition profile. Its relatively moderate ΔE value (4.16 eV), together with the global softness value, suggests enhanced molecular softness and favourable charge-transfer properties, which provide evidence of efficient σ-donation from the amino nitrogen, amide oxygen atoms, and π-d interactions of the aromatic structure. Notably, the adsorption energy of DOF (−165.16 kcal/mol) is quite significantly lower than the adsorption energies of simple amino-benzamide and benzimidazole derivatives, and in the range of strong but stable physico-chemical adsorption. The enhanced performance of DOF can be attributed to its dual amino substitutions and amide functionality, which collectively promote electronic delocalisation, multidentate surface interactions, and dispersion-driven stabilisation, as corroborated by QTAIM and NCI analyses discussed in subsequent sections. The synergistic interactions among the different functional motifs give DOF an advantage over inhibitors that uses a single functional motif and are much more susceptible to steric perturbation.

Therefore, the comparative analysis in Table 7 demonstrates a clear advantage of DOF over some reported benzamide-based inhibitors, supporting the rationality of the molecular design and underscoring its high theoretical potential for corrosion inhibition. The integrated DFT-QTAIM-NCI-Monte Carlo framework is yet another benchmark that supports its use as a useful instrument for rational inhibitor screening and design. The workflow diagram to illustrate the separation and complementarity of molecular DFT and surface MC simulation is shown in Figure 7.

CONCLUSION

In this study, the corrosion inhibition potential of 4-amino-N-(4-aminophenyl)benzamide (DOF) toward the Fe(110) surface was comprehensively evaluated using density functional theory (DFT), topological electron-density analyses, non-covalent interaction (NCI) mapping, and Monte Carlo (MC) simulations. DFT results revealed that DOF exhibits significant electronic properties favourable for adsorption. The molecule in solvent phase exhibited a HOMO energy of -5.31 eV, a LUMO energy of -1.14 eV, and an energy gap (ΔE) of 4.16 eV, indicating a moderate level of reactivity conducive to chemisorption. The chemical hardness (η = 2.08 eV) and softness (σ = 0.24 eV) further supported the molecule's ability to reorganize its electron cloud during interaction with the metal. The negative chemical potential (μ = -3.23 eV) and a relatively high electrophilicity index (ω = 2.50 eV) suggest that DOF can efficiently accept electron density from Fe and donate it back through its aromatic π-systems, stabilising the inhibitor-metal interface. Topological analysis using QTAIM confirmed the presence of stabilising intermolecular interactions. Bond critical points (BCPs) revealed moderate electron densities, such as $\rho_{(r)}$ = 0.012-0.018 a.u, and positive Laplacians ($\nabla^2\rho_{(r)}$ = 0.054-0.062 a.u) typical of closed-shell interactions (hydrogen bonding and electrostatic attraction). The negative values of $V_{(r)}$ and the ratio $G_{(r)}/V_{(r)} < 1$ established that these interactions possess partial covalent character, reinforcing the idea that DOF adsorbs through a mixed physico-chemical mechanism. NCI surface maps further validated the presence of broad green isosurfaces surrounding the aromatic rings and heteroatoms, confirming van der Waals forces, π-stacking tendencies, and localised hydrogen-bond networks. Monte Carlo simulations on the Fe(110) surface provided quantitative confirmation of strong inhibitor performance. DOF exhibited a very favourable adsorption energy of -165.16 kcal/mol, with a rigid adsorption energy of -165.45 kcal/mol and an extremely small deformation energy of 0.29 kcal/mol. This indicates that DOF adheres strongly to the steel surface with minimal structural distortion. The negative total energy of -127.65 kcal/mol further confirms thermodynamically stable adsorption. The pronounced adsorption energy and the mixed physico-chemical interactions highlight the role of dual amino substitution in enhancing surface anchoring and electronic delocalisation. While the findings indicate significant theoretical inhibition potential, experimental electrochemical validation and extended molecular dynamics simulations are required to fully establish practical performance under dynamic corrosion conditions. Nonetheless, this study provides a rigorous, mechanistically grounded, and reproducible computational framework that bridges molecular electronic structure with macroscopic adsorption behaviour. The insights derived offer actionable design principles for the rational development of advanced

benzamide-based corrosion inhibitors with improved efficiency and stability in aggressive environments.

FUTURE WORK DIRECTION

While the present study provides detailed theoretical insight into DOF adsorption, certain limitations were identified. Molecular DFT calculations rely on implicit solvent models and do not capture explicit solvent dynamics. Monte Carlo simulations employ classical force fields and do not account for time-dependent diffusion effects that molecular dynamics simulations can capture. Additionally, no experimental electrochemical validation was presented. These limitations define clear directions for future work.

REFERENCES

Adrion, D. M., & Lopez, S. A. (2022). Cross-conjugation controls the stabilities and photophysical properties of heteroazoarene photoswitches. *Organic & Biomolecular Chemistry, 20*(30), 5989–5998. [Crossref]

Anadebe, V. C., Lgaz, H., Aldalbahi, A., Lee, H., Mathias, G. E., Badeji, A. A., Thakur, A., & Ebenso, E. E. (2025). Interfacial inhibition of mild steel corrosion by Abemaciclib and Abrocitinib in acidic media: Insights from density functional theory and molecular dynamics simulations. *ChemistrySelect, 10*(32), e03502. [Crossref]

Axthammer, Q. J., Klapötke, T. M., Krumm, B., & Reith, T. (2016). Energetic Sila-Nitrocarbamates: Silicon analogues of neo-pentane derivatives. *Inorganic Chemistry, 55*(9), 4683–4692. [Crossref]

Azeez, Y. H., Mamand, D. M., Omer, R. A., Awla, A. H., & Omar, K. A. (2024). Investigation of corrosion inhibition and adsorption properties of quinoxaline derivatives on metal surfaces through DFT and Monte Carlo simulations. *Corrosion Reviews, 42*(6), 775–793. [Crossref]

Badeji, A. A. (2025). Benzotrithiophene derivative as a corrosion inhibitor: Insights from density functional theory and Monte Carlo simulation studies. *Journal of Science and Information Technology, 15*(1), 10–22.

Badeji, A. A., Omoniyi, M. T., Ogunbayo, T. B., Oladipo, S. D., & Akinbulu, I. A. (2024). Quantum chemical investigation of the degradation of acid orange 7 by different oxidants. *Discover Chemistry, 1*(1), 55. [Crossref]

Badeji, A. A., Pathmanathan, K., Abdulhussain, M. A., Hossain, I., & Runde, M. (2026). Insights into the tunability of SrHI matlockite and its group 4 transition metal-doped derivatives (TiHI, ZrHI, HfHI) for advanced electronic, photocatalytic, optoelectronic, and hydrogen storage applications: First-Principles calculations. *Materials Chemistry and Physics, 348*, 131533. [Crossref]

Badeji, A. A., Pathmanathan, K., Abdullah, H. Y., Hossain, I., & Runde, M. (2025). Unveiling the catalytic versatility of transition metal-doped coal char systems for hydrogen evolution reaction: A first-principles approach. *Chemical Physics*, 112882. [Crossref]

Bakheit, A. H., Abuelizz, H. A., & Al-Salahi, R. (2023). A DFT study and Hirshfeld surface analysis of the molecular structures, radical scavenging abilities and ADMET properties of 2-Methylthio(methylsulfonyl)-[1,2,4]triazolo [1,5-a]quinazolines: Guidance for antioxidant drug design. *Crystals, 13*(7), 1086. [Crossref]

Becke, A. D. (1993). Density-functional thermochemistry. III. The role of exact exchange. *The Journal of Chemical Physics, 98*(7), 5648–5652. [Crossref]

Bender, R., Féron, D., Mills, D., Ritter, S., Bäßler, R., Bettge, D., De Graeve, I., Dugstad, A., Grassini, S., & Hack, T. (2022). Corrosion challenges towards a sustainable society. *Materials and Corrosion, 73*(11), 1730–1751. [Crossref]

Bhatia, M. (2024). An overview of conceptual-DFT based insights into global chemical reactivity of volatile sulfur compounds (VSCs). *Computational Toxicology, 29*, 100295. [Crossref]

Boughoues, Y., Benamira, M., Messaadia, L., Bouider, N., & Abdelaziz, S. (2020). Experimental and theoretical investigations of four amine derivatives as effective corrosion inhibitors for mild steel in HCl medium. *RSC Advances, 10*(40), 24145–24158. [Crossref]

Boyd, P. G., Moosavi, S. M., Witman, M., & Smit, B. (2017). Force-Field Prediction of Materials Properties in Metal-Organic Frameworks. *The Journal of Physical Chemistry Letters, 8*(2), 357–363. [Crossref]

Carranza, M. S. S., Reyes, Y. I. A., Gonzales, E. C., Arcon, D. P., & Franco, F. C. (2021). Electrochemical and quantum mechanical investigation of various small molecule organic compounds as corrosion inhibitors in mild steel. *Heliyon, 7*(9), e07952. [Crossref]

Cho, D., Ko, K. C., Ikabata, Y., Wakayama, K., Yoshikawa, T., Nakai, H., & Lee, J. Y. (2015). Effect of Hartree-Fock exact exchange on intramolecular magnetic coupling constants of organic diradicals. *The Journal of Chemical Physics, 142*(2). [Crossref]

Demir, S., Tinmaz, F., Dege, N., & Ilhan, I. O. (2016). Vibrational spectroscopic studies, NMR, HOMO-LUMO, NLO and NBO analysis of 1-(2-nitrobenzoyl)-3,5-diphenyl-4,5-dihydro-1 H -pyrazole with use X-ray diffractions and DFT calculations. *Journal of Molecular Structure, 1108*, 637–648. [Crossref]

Ebenso, E. E., Verma, C., Olasunkanmi, L. O., Akpan, E. D., Verma, D. K., Lgaz, H., Guo, L., Kaya, S., & Quraishi, M. A. (2021). Molecular modelling of compounds used for corrosion inhibition studies: A review. *Physical Chemistry Chemical Physics, 23*(36), 19987–20027. [Crossref]

El-Hendawy, M. M., Kamel, A. M., & Mohamed, M. M. A. (2022). The anti-corrosive behavior of benzo-fused N-heterocycles: An in silico study toward developing organic corrosion inhibitors. *Physical Chemistry Chemical Physics, 24*(2), 743–756. [Crossref]

Fatemeh Mollaamin & Majid Monajjemi. (2023). Coating of Al-X (X = Mg, Ga, Si) alloys nanosurface with organic corrosion inhibitors using TD-DFT approach: Intra-atomic and interatomic investigation through Langmuir adsorption study. *Russian Journal of Physical Chemistry A, 97*(10), 2241–2257. [Crossref]

Fouda, A. E., & Besley, N. A. (2018). Assessment of basis sets for density functional theory-based calculations of core-electron spectroscopies. *Theoretical Chemistry Accounts, 137*(1), 6. [Crossref]

Frisch, M., Trucks, G., Schlegel, H., Scuseria, G., Robb, M., Cheeseman, J., Scalmani, G., Barone, V., Petersson, G., & Nakatsuji, H. (2016). *Gaussian 16 Revision C. 01, 2016*. Gaussian Inc.

Fung, V., Hu, G., Ganesh, P., & Sumpter, B. G. (2021). Machine learned features from density of states for accurate adsorption energy prediction. *Nature Communications, 12*(1), 88. [Crossref]

Gelb, L. D., & Müller, E. A. (2002). Location of phase equilibria by temperature-quench molecular dynamics simulations. *Fluid Phase Equilibria, 203*(1–2), 1–14. [Crossref]

Hamidi, H., Shojaei, F., Pourfath, M., & Vaez-Zadeh, M. (2024). Adsorption behavior of some green corrosion inhibitors on Fe (110) surface: The critical role of d-π interactions in binding strength. *Applied Surface Science, 655*, 159425. [Crossref]

Haritha, M., & Suresh, C. H. (2024). Unveiling drug discovery insights through molecular electrostatic potential analysis. *WIREs Computational Molecular Science, 14*(6), e1735. [Crossref]

Heard, C. J., Čejka, J., Opanasenko, M., Nachtigall, P., Centi, G., & Perathoner, S. (2019). 2D oxide nanomaterials to address the energy transition and catalysis. *Advanced Materials, 31*(3), 1801712. [Crossref]

Hegazy, A. M., Haiba, N. S., Awad, M. K., & Mahgoub, F. M. (2023). Synthesis, DFT, molecular dynamics, and Monte Carlo simulation of a novel thiourea derivative with extraordinary inhibitive properties for mild steel in 0.5 M sulphuric acid. *Physical Chemistry Chemical Physics, 25*(13), 9532–9547. [Crossref]

Humphrey, W., Dalke, A., & Schulten, K. (1996). VMD: Visual molecular dynamics. *Journal of Molecular Graphics, 14*(1), 33–38. [Crossref]

Iravani, D., Esmaeili, N., Akbarinezhad, E., Berisha, A., & Mehmeti, V. (2025). Influence of Donor and Acceptor Groups on the Inhibition Performance of Benzamide Derivatives in CO2-Saturated Media: Experimental and Theoretical Researches. *Journal of Materials Engineering and Performance, 34*(18), 20787–20805. [Crossref]

Jay, R. M., Banerjee, A., Reinhard, M., Zhao, H., Huse, N., Gaffney, K. J., Kroll, T., Sokaras, D., & Wernet, P. (2025). Metal-ligand covalency of C-H activating iridium complexes from L-edge valence-to-core resonant inelastic X-ray scattering. *Chemistry*. [Crossref]

Jiang, Z., Deng, S., Qiang, Y., Xu, J., Shao, D., & Li, X. (2024). Thiourea derivatives as efficient inhibitors for the corrosion of cold rolled steel in citric acid solution: Experimental and computational studies. *Journal of Molecular Structure, 1318*, 139218. [Crossref]

Kalwar, B. A., Fangzong, W., Soomro, A. M., Naich, M. R., Saeed, M. H., & Ahmed, I. (2022). Highly sensitive work function type room temperature gas sensor based on Ti doped hBN monolayer for sensing CO2 , CO, H2 S, HF and NO. A DFT study. *RSC Advances, 12*(53), 34185–34199. [Crossref]

Kasprzhitskii, A., & Lazorenko, G. (2021). Corrosion inhibition properties of small peptides: DFT and Monte Carlo simulation studies. *Journal of Molecular Liquids, 331*, 115782. [Crossref]

Kaya, S. (2025). Conceptual density functional theory-based applications in extraction studies. In *Green analytical chemistry* (pp. 43–58). Elsevier. [Crossref]

Koopmans, T. (1934). About the assignment of wave functions and eigenvalues to the individual electrons of an atom. *Physica, 1*(1–6), 104–113. [Crossref]

Krosschell, R. D., Hensen, E. J., & Filot, I. A. (2024). Unravelling CO activation on flat and stepped Co surfaces: A molecular orbital analysis. *The Journal of Physical Chemistry C, 128*(22), 8947–8960. [Crossref]

Kumar, B., Devi, J., Dubey, A., Tufail, A., & Arora, T. (2023). Inspecting the anti-tuberculosis, antimicrobial, and anti-inflammatory efficiency of newly synthesized Co (II), Ni (II), Cu (II) and Zn (II) complexes of hydrazone ligands: Characterization and computational studies. *Applied Organometallic Chemistry, 37*(12), e7291. [Crossref]

Le Minh Pham, T., Khoa Phung, T., & Viet Thang, H. (2022). DFT insights into the adsorption mechanism of five-membered aromatic heterocycles containing N, O, or S on Fe(1 1 0) surface. *Applied Surface Science, 583*, 152524. [Crossref]

Liao, X., Lu, R., Xia, L., Liu, Q., Wang, H., Zhao, K., Wang, Z., & Zhao, Y. (2022a). Density functional theory for electrocatalysis. *Energy & Environmental Materials, 5*(1), 157–185. [Crossref]

Liao, X., Lu, R., Xia, L., Liu, Q., Wang, H., Zhao, K., Wang, Z., & Zhao, Y. (2022b). Density functional theory for electrocatalysis. *Energy & Environmental Materials, 5*(1), 157–185. [Crossref]

Lu, T., & Chen, F. (2012). Multiwfn: A multifunctional wavefunction analyzer. *Journal of Computational Chemistry, 33*(5), 580–592. [Crossref]

Lu, T., Chen, R., Liu, Q., Zhong, Y., Lei, F., & Zeng, Z. (2024). Unveiling the nature and strength of selenium-centered chalcogen bonds in binary complexes of SeO2 with oxygen-/sulfur-containing Lewis bases: Insights from theoretical calculations. *International Journal of Molecular Sciences, 25*(11), 5609. [Crossref]

Mamand, D. M., Azeez, Y. H., & Qadr, H. M. (2023). Monte Carlo and DFT calculations on the corrosion inhibition efficiency of some benzimide molecules. *Mongolian Journal of Chemistry, 24*(50), 1–10. [Crossref]

Mamand, D. M., Kak Anwer, T. M., & Qadr, H. M. (2024). Corrosion inhibition performance of organic compounds and theoretical calculations based on density functional theory (DFT). *Corrosion Reviews, 42*(1), 1–15. [Crossref]

Mancuso, J. L., Mroz, A. M., Le, K. N., & Hendon, C. H. (2020). Electronic structure modeling of metal-organic frameworks. *Chemical Reviews, 120*(16), 8641–8715. [Crossref]

Marenich, A. V., Cramer, C. J., & Truhlar, D. G. (2009). Universal solvation model based on solute electron density and on a continuum model of the solvent defined by the bulk dielectric constant and atomic surface tensions. *The Journal of Physical Chemistry B, 113*(18), 6378–6396. [Crossref]

Martín Pendás, Á., & Contreras-García, J. (2023). Weak interactions. In Á. Martín Pendás & J. Contreras-García, *Topological approaches to the chemical bond* (pp. 175–218). Springer International Publishing. [Crossref]

Meunier, M., & Robertson, S. (2021). Materials Studio 20th anniversary. *Molecular Simulation, 47*(7), 537–539. [Crossref]

Mishra, A., Verma, C., Lgaz, H., Srivastava, V., Quraishi, M. A., & Ebenso, E. E. (2018a). Synthesis, characterization and corrosion inhibition studies of N-phenyl-benzamides on the acidic corrosion of mild steel: Experimental and computational studies. *Journal of Molecular Liquids, 251*, 317–332. [Crossref]

Mishra, A., Verma, C., Lgaz, H., Srivastava, V., Quraishi, M. A., & Ebenso, E. E. (2018b). Synthesis, characterization and corrosion inhibition studies of N-phenyl-benzamides on the acidic corrosion of mild steel: Experimental and computational studies. *Journal of Molecular Liquids, 251*, 317–332. [Crossref]

Moberly, J. G., Bernards, M. T., & Waynant, K. V. (2018). Key features and updates for origin 2018. *Journal of Cheminformatics, 10*(1), 5. [Crossref]

Mojica-Sánchez, J. P. (2023). Applications of the quantum theory of atoms in molecules in chemical reactivity. In *Chemical reactivity* (pp. 1–14). Elsevier. [Crossref]

Murmu, M., Murmu, N. C., Ghosh, M., & Banerjee, P. (2022). Density functional theory, Monte Carlo simulation and non-covalent interaction study for exploring the adsorption and corrosion inhibiting property of double azomethine functionalised organic molecules. *Journal of Adhesion Science and Technology, 36*(23–24), 2732–2760. [Crossref]

Muthamma, K., Kumari, P., Lavanya, M., & Rao, S. A. (2021). Corrosion inhibition of mild steel in acidic media by N-[(3,4-dimethoxyphenyl)methyleneamino]-4-hydroxy-benzamide. *Journal of Bio- and Tribo-Corrosion, 7*(1), 10. [Crossref]

Nelson, F. A., Badeji, A. A., Emmanuel, E., & Louis, H. (2025). SrHX (X = Cl, Br, I) matlockite-type hydrides: A DFT study and its application for optoelectronics, hydrogen storage, and photocatalysis. *International Journal of Hydrogen Energy, 193*, 152378. [Crossref]

Odeyemi, O. O., & Alaba, P. A. (2025). Efficient and reliable corrosion control for subsea assets: Challenges in the design and testing of corrosion probes in aggressive marine environments. *Corrosion Reviews, 43*(1), 79–126. [Crossref]

Oladipo, S. D., Akinpelu, O. I., & Omondi, B. (2023). Ligand-guided investigation of a series of formamidine-based thiuram disulfides as potential dual-inhibitors of COX-1 and COX-2. *Chemistry & Biodiversity, 20*(1), e202200875. [Crossref]

Oladipo, S. D., Luckay, R. C., Olalekan, S. O., Badeji, A. A., Yusuf, T. L., Adeleke, A. A., & Matinise, N. (2025). Probing the inhibitory potential of halogenated symmetrical formamidine against MAO-A and MAO-B: Structural elucidation, molecular dynamic simulation and DFT computational studies. *Chemistry & Biodiversity*, e00886. [Crossref]

Oliveira, J. R., Kotzebue, L. R. V., Ribeiro, F. W. M., Mota, B. C., Zampieri, D., Mazzetto, S. E., Ishida, H., & Lomonaco, D. (2017). Microwave-assisted solvent-free synthesis of novel benzoxazines: A faster and environmentally friendly route to the development of bio-based thermosetting resins. *Journal of Polymer Science Part A: Polymer Chemistry, 55*(21), 3534–3544. [Crossref]

Othman, K. A., Hamad, W. M., & Omer, R. A. (2025). Theoretical and experimental exploration of organic molecules adsorption on iron surfaces for corrosion inhibition: A review. *Corrosion Reviews, 43*(3), 335–359. [Crossref]

Othman, N., Azhar, N., Megat Abdul Rani, P. S., & Mohamed Zaini, H. (2016). Metal removal and antimicrobial properties of watermelon rind modified with clove. *MATEC Web of Conferences, 78*, 01028. [Crossref]

Oyeneyin, O. E., Ojo, N. D., Ipinloju, N., Agbaffa, E. B., & Emmanuel, A. V. (2022). Investigation of the corrosion inhibition potentials of some 2-(4-(substituted)arylidene)-1H-indene-1,3-dione derivatives: Density functional theory and molecular dynamics simulation. *Beni-Suef University Journal of Basic and Applied Sciences, 11*(1), 132. [Crossref]

Popelier, P. L. (2016). Quantum chemical topology. In *The chemical bond II: 100 years old and getting stronger* (pp. 71–117). Springer. [Crossref]

Rai Deka, J. K., Sahariah, B., & Sarma, B. K. (2024). Understanding the cis-trans amide bond isomerization of N , N '-diacylhydrazines to develop guidelines for a priori prediction of their most stable solution conformers. *The Journal of Organic Chemistry, 89*(15), 10419–10433. [Crossref]

Schlegel, J. (2023). *The world of steel: On the history, production and use of a basic material*. Springer Fachmedien Wiesbaden. [Crossref]

Taghavikish, M., Dutta, N., & Roy Choudhury, N. (2017). Emerging corrosion inhibitors for interfacial coating. *Coatings, 7*(12), 217. [Crossref]

Tsuji, T., Machida, Y., Feyter, S. D., Tahara, K., & Tobe, Y. (2025). Multiguest-induced structural switching in a self-assembled monolayer network at the liquid-solid interface. *The Journal of Physical Chemistry C, 129*(16), 7894–7902. [Crossref]

Wang, B., Yao, P., Zhang, J., Su, Y., Zhou, M., & Li, E. (2025). Imidazole-based ionic liquids' ability to suppress corrosion and adsorb 1mol/L Hcl on the surface of mild steel: Production, electrochemistry, surface investigation, and theoretical computations. *SSRN*. [Crossref]

Weinhold, F. (2012). Natural bond orbital analysis: A critical overview of relationships to alternative bonding perspectives. *Journal of Computational Chemistry, 33*(30), 2363–2379. [Crossref]

Zainab, S., Ashraf, A., Siddiqui, W. A., Raza, M. A., Niaz, S., Arshad, J. Z., Arshad, M. N., Aman, F., Sandhu, Z. A., & Asiri, A. M. (2024). Piroxicam analogue metal complexes: Synthesis, crystal structures, molecular modeling and biological studies. *Applied Organometallic Chemistry, 38*(7), e7481. [Crossref]

Zhang, W., Liu, Y., Zhang, Y., Wang, L.-J., Wu, Y.-C., & Li, H.-J. (2020). 9-Substituted acridines as effective corrosion inhibitors for mild steel: Electrochemical, surface morphology, and computational studies. *New Journal of Chemistry, 44*(16), 6464–6474. [Crossref]

Zheng, J., Lu, Z., Wu, K., Ning, G.-H., & Li, D. (2020). Coinage-metal-based cyclic trinuclear complexes with metal-metal interactions: Theories to experiments and structures to functions. *Chemical Reviews, 120*(17), 9675–9742. [Crossref]

Zhurko, G. A., & Zhurko, D. A. (2005). *Chemcraft-graphical program for visualization of quantum chemistry computations*. Ivanovo, Russia.